

Facile patterning of genetically engineered M13 bacteriophage for directional growth of human fibroblast cells†

So Young Yoo,‡ Woo-Jae Chung,‡ Tae Hyun Kim,§ Mimi Le and Seung-Wuk Lee*

Received 28th August 2010, Accepted 28th October 2010

DOI: 10.1039/c0sm00879f

We report a facile strategy for the patterning of cells that utilizes nanofibrous RGD-engineered phages in conjunction with micro-contact printing methods to provide human fibroblast cells with specific biochemical and physical cues. This approach can be used for high-throughput screening assays as well as for energy and biosensor development.

Introduction

Fabrication of precisely designed active biomaterials is of great interest in many areas of bionanotechnology including regenerative medicine, drug screening, and biosensors.^{1–7} Micro- and nanometre scale defined patterns have been developed which can control the spacing and density of signaling molecules through top-down microfabrication approaches, such as photolithography, e-beam lithography, and microcontact printing techniques.^{2,7–9} Recently developed bottom-up biomaterials such as peptide amphiphiles,^{10–12} and polymers^{1,13–15} or protein matrices^{16,17} can more closely mimic the nanofibrous network structures of extracellular matrices. Together with the physical structures, additional control of biochemical ligands, signaling density, and dynamic degradation or cross-linking have been considered as critical components to instruct target cells to assume desired tissue morphologies and fates.^{10,17–19}

Recently, our group and others utilized filamentous viral particles as tissue regenerating materials following genetic and chemical modification.^{20–23} Specifically, our group utilized the unique ability of M13 phage to self-replicate, self-assemble and self-evolve to prepare various tissue-like scaffold structures for tissue regeneration. Through the insertion of a desired gene sequence, we could easily display high densities (1.5×10^{13} epitopes per cm^2) of signaling peptides along the nanofiber-like phage surfaces. Due to the long-rod shape and monodispersity of the phage, we were able to fabricate various two-dimensional or three-dimensional self-aligned structures organized from the nanometre scale to the centimetre scale without any nano- or microfabrication processes. The resulting structures can control physical and chemical cues to direct the growth of desired cells, including neural cells, preosteoblasts, fibroblasts and others.^{20,24,25}

Phage-based patterning has previously been used in the nanofabrication of electronic or energy storage devices.^{26–29} However, if one can couple such biologically active phage materials with microfabrication techniques, it will become possible to construct versatile platforms for various biomedical applications, such as tissue regeneration, drug screening, and biological assay test-beds to investigate the various parameters for cell biological processes.

Here, we developed a facile methodology to pattern engineered phage for directional guidance of human fibroblasts for tissue engineering and bioassay applications. We employed polydimethylsiloxane (PDMS) microcontact printing techniques to prepare the micropatterned phage structures for guiding directional growth of human fibroblasts. We also demonstrated that nanofibrous structures, along with the biochemical signals presented by the phage microstructures, are critical to guiding human fibroblasts to grow desired elongated morphologies. Our hybrid bottom-up and top-down approach can be useful not only for regenerative medicine and high-throughput screening assays, but also for other applications including biosensors, energy, and semiconductor development.

Results and discussion

We fabricated patterned selective phage surfaces using microcontact printing approaches with PDMS stamps (Fig. 1). We utilized the engineered M13 phage with integrin-binding peptide (RGD), which was constructed through directed evolutionary cloning approaches previously reported.^{20,21} In order to create the desired phage patterns, we first deposited a non-polar self-assembled monolayer (SAM) of 1-octadecanethiol (ODT) on gold substrates using PDMS stamps, and followed with deposition of a cysteamine SAM by dipping the substrate in cysteamine solution. Selective patterning of hydrophobic ODT and hydrophilic cysteamine induces selective M13 phage patterning on hydrophilic surface regions, where the RGD-modified phage serves as a nanofibrous platform to guide directional cell growth.

We fabricated two patterns with different spacing (5/10 and 10/20 μm for cysteamine and ODT respectively). We chose 5/10 and 10/20 μm spacing because this scale might be relevant to the size of the human fibroblasts and significantly affects the cell morphology. AFM analyses showed that we could fabricate the controlled spacing of these selective patterns (Fig. 2A) by sequential deposition of the ODT and cysteamine on the gold substrates. After applying the phage suspension ($0.1\text{--}1 \text{ mg mL}^{-1}$) for 60 min, followed by sequential washing using DI water, we could obtain selective deposition of the phage on cysteamine patterned areas as shown using AFM (Fig. 2B). After ODT deposition, the average height increased to $\sim 2 \text{ nm}$, measured by AFM (Fig. 2A). Height changes ($\sim 7 \text{ nm}$) after deposition of phage imply the selective deposition of phage on cysteamine areas, which are partly composed of cysteamine coatings of

1-220 Donner Lab, Bioengineering, University of California, Berkeley, Physical Biosciences Division, Lawrence Berkeley National Laboratory, Berkeley Nanoscience and Nanoengineering Institute, Berkeley, CA, 94720, USA. E-mail: leesw@berkeley.edu; Fax: +1-510-486-6488; Tel: +1-510-486-4628

† Electronic supplementary information (ESI) available: Human fibroblasts on the control substrate. See DOI: 10.1039/c0sm00879f

‡ Both authors contributed equally to this work.

§ Current address: Department of Chemistry, Soonchunhyang University, Asan 336-745, South Korea.

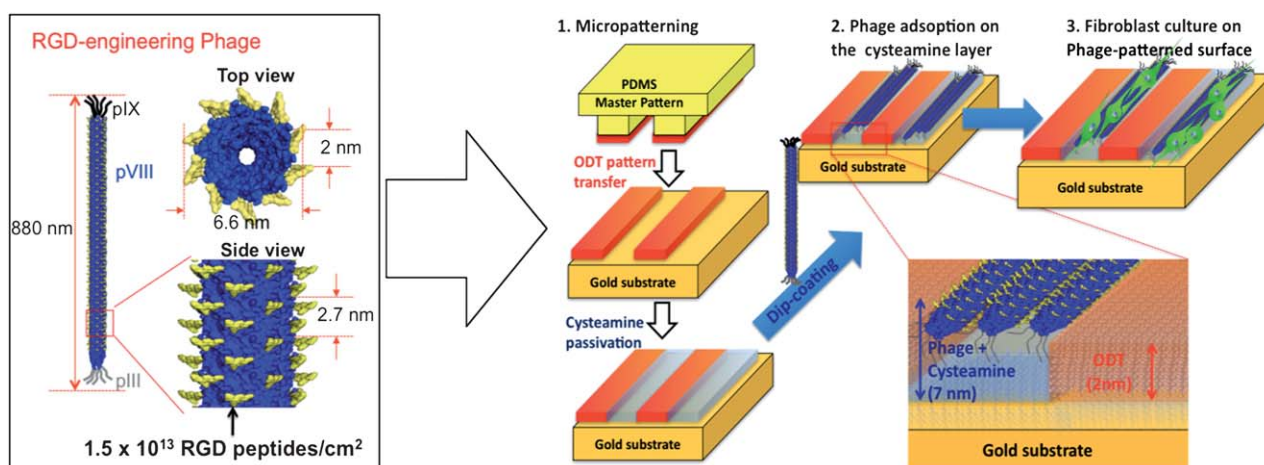


Fig. 1 Schematic illustration of phage engineering and selective phage patterning for directional growth of human fibroblast cells. M13 phage was genetically engineered to display integrin-binding motif RGD on every copy of pVIII major coat proteins. We used the resulting engineered M13 phage to create micropatterned surfaces using microfabrication techniques. We first used PDMS microcontact printing to create hydrophobic 1-octadecanethiol (ODT) patterned surfaces. We then coated the substrate with hydrophilic cysteamine to create a self-assembled monolayer (SAM). When the patterned substrate is submerged in M13 phage suspension and pulled through dip-coating methods, phages are selectively deposited on hydrophilic cysteamine coated areas. These patterned substrates were then used for guiding directional cell growth.

0.5–0.8 nm thick (Fig. 2B). AFM and fluorescent images showed selective and homogeneous deposition of phage on the desired micropatterned substrates (Fig. 2C, S1 and S2 in ESI†). In order to obtain these phage coatings, we tested and optimized phage patterning by varying the concentrations of phages (0.01 – 1 mg mL⁻¹), incubation times (5 min to overnight) and/or pulling speed (10 – 100 $\mu\text{m min}^{-1}$) to fabricate uniformly patterned phage structure. Due to the convective flow of phage suspension toward the hydrophilic region from the hydrophobic background, along with the downward movement of the meniscus during the drying process at the contact line, phage deposition on hydrophilic stripe patterns leads to bimodal alignment of the phage fibers along the strips. Horizontal or diagonal orientation of phage fibers was formed along the central axis of the vertical hydrophilic stripes. Because of the dominant effect from the hydrophobic background on the meniscus movement, only

small amounts of phage were deposited on the hydrophilic cysteamine area (thickness is ~ 7 nm). Instead, phages applied on the substrate without such hydrophobic/hydrophilic patterns formed much thicker phage deposition in similar conditions (data not shown). 1 mg mL⁻¹ phage concentration and 10 $\mu\text{m min}^{-1}$ pulling speed gave the most optimized uniform phage coverage (Fig. S1 and S2†). Higher speed gave narrower patterning whereas lower speed gave wider patterning on hydrophilic surfaces due to hydrophobic repulsion from the next hydrophobic regions. We believe that M13 phages were selectively deposited on hydrophilic cysteamine surfaces through hydrophilic and electrostatic interaction as well as by hydrophobic repulsion generated by the nearby hydrophobic ODT. The resulting nanofibrous patterns, with a high-density of RGD-peptides on the phage, were further investigated for inducing specific cellular responses.

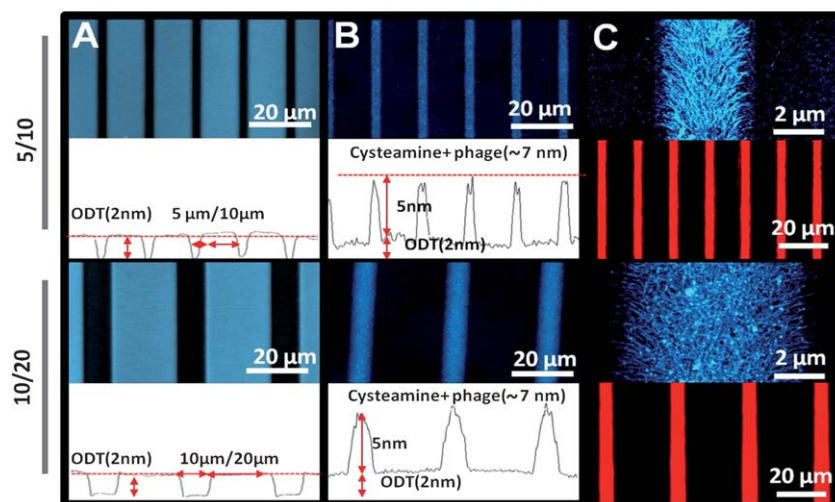


Fig. 2 Micro patterning of M13 phage. (A) AFM image of cysteamine (Au)/ODT SAM pattern. (B) AFM image of selective adsorption of M13 phage on the desired micropattern. (C) Magnified AFM (of B) and fluorescent images of patterned M13 phage on the gold substrates. (Up: 5 $\mu\text{m Au}/10$ $\mu\text{m ODT}$, down: 10 $\mu\text{m Au}/20$ $\mu\text{m ODT}$; fluorescent image stained with anti-fd phage.)

The micropatterned substrates with integrin-binding RGD-peptide engineered phage exerted specific cellular effects on cultured human fibroblasts. We chose human fibroblast cells (CCD32Sk) because of their known sensitivity to textured materials,^{30–33} and because directional guidance is important to regenerate desired tissue morphologies during wound healing processes.³⁴ When fibroblast cells were cultured on top of RGD-phage patterned surfaces, the cells attached well and elongated through the direction of the phage pattern (Fig. 3A and B). Cell alignment on the selectively deposited phage regions was maintained during cell proliferation for up to eight days (data not shown). The specific biochemical effect of the RGD-phage was further observed by using RGE- and wildtype-control phage-patterned substrates (Fig. 3C and D and see Fig. S4A†). When RGE- and wildtype-phage were used, the attached number of cells were much less and the elongation of the fibroblasts were much shorter than those observed on the RGD-phage. However, the attached fibroblast cells on the RGE-phage patterned substrates still exhibited aligned morphology through the line pattern direction. Interestingly, the center of the fibroblasts was on the boundary of the patterned substrate (white arrows in Fig. 3D), while that of the RGD substrate was mainly in the middle of the phage patterns (white arrow in Fig. 3B). We believe that the resulting elongated cell morphology from the RGE-phage patterns was mainly caused by the topological edge structures generated by the phage patterning, because many cells can sense micro ridge or groove structures.^{6,13,19} ODT/cysteamine patterns might induce similar topological edge effects as observed with the RGE-edge. However, we could not find such parallel elongation patterns as those shown in our control experiments with RGE-phage edge effects (data not shown). We believe that this morphological difference might come from height difference between ODT and the deposited phages. The topological height difference of ODT/cysteamine is 1.2–1.5 nm, whereas that of the ODT/RGE-phage patterns is ~ 5 nm.

In order to confirm the importance of the specific physical or chemical cue effects of the nanofibrous phage structures, we performed additional control experiments using RGD-peptide (Fig. 3E) or phage without micropatterns. We first synthesized a linear RGD peptide linked through a glycine linker and cysteine (RGDGGGC) using Fmoc chemistry, where cysteine binds to Au surfaces and GGG provides spacing of the RGD-peptide. After PDMS micro-contact printing of the RGD-peptides, we achieved the self-assembled monolayers of the RGD-peptides which display the same signaling peptides but without the nanofibrous structures of the RGD-phage. AFM studies (Fig. S3A†) showed that the RGD-peptide generated relatively uniform self-assembled monolayers with average height of ~ 2 nm (Fig. S3B†) and with lower surface roughness (1.53 ± 0.37 nm) than those of phage patterns (3.46 ± 0.53 nm). The resulting RGD-peptide patterns could induce directional growth of the fibroblasts. However, the cells exhibited shorter elongation and less alignment than those on the RGD-phage patterned substrates. We believe that the different morphologies of the RGD-peptide patterns compared with RGD-phage patterns might come from the topological changes, such as edge structures made by its fibrous textures, and more surface areas generated by the nanofibrous phage patterns.

In addition, when the cells were cultured on the drop-cast phage films without micropatterns (Fig. 3G), the cells adhered well and exhibited less elongated morphology. We also observed locally aligned fibroblast growth within ~ 200 to $300 \mu\text{m}$ domain, which might be induced by local lyotropic liquid crystalline ordered phage

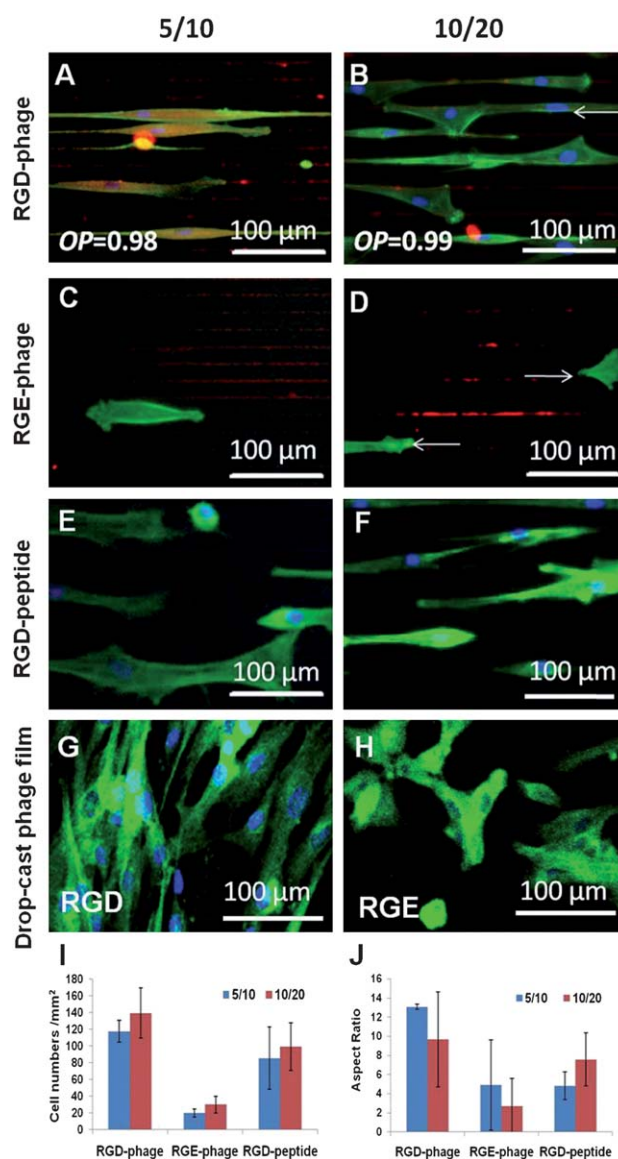


Fig. 3 Human fibroblast morphologies on the phage patterned surfaces. (A and B) Cellular morphologies from RGD-, (C and D) RGE-phage, (E and F) RGD-peptide (RGDGGGC) patterned substrates and (G) RGD-, (H) RGE-phage drop cast films. (A, C, and E: $5 \mu\text{m}$ cysteamine/ $10 \mu\text{m}$ ODT patterns; B, D, and F: $10 \mu\text{m}$ cysteamine/ $20 \mu\text{m}$ ODT patterns.) The fluorescent images were labeled with phalloidin for actin (green), DAPI for nucleus (blue), phage antibody for phage (red). Characterization of morphological parameters of the cellular response for the phage substrates in cell numbers (I) and aspect ratio (J).

films. However, the overall orientation of fibroblasts is a random collection of the locally oriented fibroblasts throughout the samples. When the cells were cultured on the RGE-phage drop cast films, the cells showed significantly decreased cell numbers and round-cell shapes, which indicated that there is little focal contact between the fibroblasts and the substrates (Fig. 3H). On ODT or gold substrate controls lacking a pattern, the fibroblasts exhibited randomly grown morphologies in no specific direction (Fig. S4†). We also observed microspacing dependent cell morphologies: The $10/20 \mu\text{m}$ RGD-phage patterned substrates had higher numbers of cells compared

with cultures on 5/10 μm patterned substrates. We believe that 10/20 μm pattern spacing provides more favorable hydrophilic surfaces for the fibroblasts than 5/10 μm patterns due to the comparable size of the human fibroblasts. Similar microspacing preferences of the fibroblasts were previously observed on micropeg pillars.³⁵ By analyzing the cellular morphology parameters (Fig. 3I and J), we quantified the effects of physical and chemical cues generated by the engineered phage on the 5/10 or 10/20 μm patterned surfaces with different phage substrates. In all quantifications of parameters including cell attachment, areas, aspect ratios, and orientation, RGD-phage patterned substrates exhibited the most favorable cellular morphologies.

We believe that the resulting preferential and desired elongated human fibroblast morphologies on the RGD-phage were mainly contributed by the biochemical and physical cues generated by the phage structure. In our phage-tissue engineering materials system, the nanofibrous phage (880 nm by 6.6 nm) uniformly displays, at high density (1.5×10^{13} ligands per cm^2), the 2700 copies of RGD-peptides uniformly, with a spacing of 2.7 nm axially, and 2 nm laterally along the phage fiber (Fig. 1). Such structures might help cells to recognize the high-density of RGD-peptide organized along the phage fiber, inducing them to form stable focal contacts on phage-coated surfaces.²⁰ Previous RGD-ligand studies showed that ligand density, ligand spacing, presentation, and their clustering play a critical role to induce specific cellular morphologies.^{36–39} Higher peptide density led to increased cell spreading, whereas cells on lower density maintained a rounder morphology. Minimal peptide concentration necessary for cell attachment and spreading was 6×10^8 ligands per cm^2 and an average peptide-to-peptide spacing of 440 nm in the case of human foreskin fibroblast culture. In addition, nanotextured morphologies enhanced cellular interaction.^{10,40} Therefore, we believe that our nanofibrous RGD-phage tissue matrices can induce similar effects as those previously observed.

We also measured the orientation and elongation of the phage to the preferential direction and calculated orientation order parameters ($\text{OP} = \frac{1}{2}(3\cos^2\theta - 1)$, with θ = measured angle of the long axis of cells in relation to the preference angle). The fibroblasts on RGD-modified phage-patterned surfaces exhibited preferential orientation through the direction of the patterned phage, with an orientation order parameter (OP) of 0.99 on 10/20 μm patterns and 0.98 on 5/10 μm patterns comparing to values for RGE-phage and RGD-peptide (OP = ~ 0.8 and ~ 0.7 respectively; OP = 1 for perfectly oriented, and 0 for randomly oriented system). These results show that the nanofibrous RGD-phage patterned substrates induce the human fibroblast cells to attach on the desired patterned substrates through the programmed RGD signaling peptide on the phage surfaces. Additionally, the RGD-phage patterned substrates encouraged elongated morphologies through nanofiber-like phage structures. We believe that the resulting structures provided the necessary physical topology with appropriate biochemical cues critical to synergic stimulation of the target cells.

Extracellular matrices (ECMs) are mainly composed of nanofibrous protein networks.^{41–44} Their fibrillar diameter ranges 3–20 nm.^{45–47} These structures provide instructive cues to nearby cells, orchestrating the assumption of desired cellular morphologies and fates in a dynamic manner through signaling ligands, hierarchically organized supramolecular structures, and material stiffness. Various approaches have been explored to recapitulate such nanofibrous cell-instructive matrices on device platforms for the purpose of tissue

regeneration, drug-screening and molecular biological assays.^{3,4,8,48} However, previous approaches based on synthetic polymers or natural protein matrices without micro- and nano-fabrication have trouble incorporating both nanofibrous network structures and controllable presentation of chemical ligands in a well-defined manner. Our phage-based patterning approaches provide multiple advantages over conventional biomaterial patterning: first, we can easily prepare basic building blocks for nanofibrous tissue scaffolds through genetic engineering and bacterial amplification. Second, we can self-assemble nanofiber micropatterns with high signaling density through facile microcontact printing techniques, which closely mimic the ECM structures. Third, we can modulate the chemical ligand structures through single or multiple mutations of deposited phage genomes, with little change of substrate physical properties, spacing, and chemical density. Fourth, the phage does not elicit any harmful or toxic response from eukaryotic cell systems, which would allow for biocompatibly tailoring of tissue structures for regenerative medicine purposes. Thus, our facile phage micropatterning approaches might be useful for various applications beyond the scope of what is demonstrated here.

In summary, a facile phage patterning method was developed by combining top-down microcontact printing with bottom-up designed genetically engineered M13 bacteriophages. We demonstrated that the periodic phage patterns could support human fibroblast cell growth and guide the growth processes of the target cells. The specific biochemical cues provided through genetic engineering of the M13 phage, in conjunction with their intrinsic nanofibrous structure, played a critical role in inducing the directional growth of the target cells. We believe that the resulting elongated cell morphology from the phage patterns was mainly caused by the topological surface structures by the nanofibrous phage, which is a key factor giving stronger directional growth of fibroblast cells on RGD-phages rather than on RGD peptide. RGD peptide gives adhesion force and stimulates cellular proliferation by interacting cells, which would be the chemical cue effect by RGD-peptide itself. The spacing (peptide density exposed to cells) together with topologic structures can also be recognized by cells and help cells to elongate more. The interspacing of M13 pVIII proteins as 2.7 nm represents the spacing of RGD peptide motifs along the filamentous phage structure (Fig. 1) and the phage particles were deposited on the pattern surface constituting three-dimensional fibrillar structures which mimics the natural extracellular matrices. We believe that nanofibrous phage structures with high density of RGD peptide together with high surface areas with topological edge will help cells more elongated along the phage pattern, which then help again cells to recognize RGD peptide better than in the case of peptide-only pattern with smooth surfaces. We quantitatively analyzed the contribution of the nanofiber-like phage structures to the cell morphological difference in terms of number of attached cells on the pattern surface and elongation of the cells along the phage stripe patterns as shown in Fig. 3I and J. The use of surfaces with defined nanoarrays of RGD peptides has been studied for the control of integrin-mediated cell adhesion and behavior.^{49,50} Along these lines, our phage nanofiber structure can support highly defined dense arrays of the integrin ligands in regular spacing with its nanofibrous topographic structures and gives the different proliferation from RGD-peptide itself application. Our novel phage patterning approach will be useful to develop various test-beds for cell biology studies, drug screening, and tissue regenerating

materials, as well as other phage nanocoatings for semiconductor, energy, and biosensor applications.

Experimental section

Genetic engineering and purification of M13 bacteriophage

M13 phage major coat protein pVIII was engineered to display the RGD or RGE peptide motif by using a partial library cloning and a site-specific mutagenesis approach as previously reported.²¹

Patterning of RGD-phage or RGD-peptide on ODT/cysteamine-patterned substrate

Phages were selectively coated on the cysteamine pattern using dip-coating method. The ODT/cysteamine patterned substrate (vertical cysteamine stripe pattern) was first immersed in the RGD-phage solution (1 mg mL⁻¹) vertically and pulled up at a controlled speed by a computer-programmed system. To find the optimal condition for selective phage deposition on the pattern, we tested the withdrawal speed in the range of 10–100 $\mu\text{m min}^{-1}$. In case of RGD peptide deposition, RGDGGGC were used, where cysteine binds to Au surfaces and GGG provides spacing of the RGD-peptide. The ODT patterned substrate was immersed in RGD peptide solution (RGDGGGC) vertically and pulled up at the same condition as phage pattern. The resulted phage or peptide pattern substrate was dried in air for 2 h and kept in a desiccator prior to use.

Human fibroblast cell culture

CCD32SK, human fibroblast cells were obtained from Cell Facilities in the University of California, Berkeley (Berkeley, CA) and used at passages 20–30. Cells were cultured in DMEM media (Invitrogen, Carlsbad, CA) with 10% heat-inactivated fetal bovine serum and 1% antibiotics–antimicrobials at 37 °C, 5% CO₂ and 95% humidity. The growth media was changed every 2 days, and the base population of cells was passaged when near confluency. After trypsinization of cells cultured as a monolayer, the cells were added onto patterned (or bare) surface at 5×10^3 cells per mL¹.

Atomic force microscopy (AFM) analysis

The topographic images of the patterned surfaces were acquired in air using AFM (MFP-3D AFM, Asylum Research, Santa Barbara, CA) operating on tapping mode with a silicon cantilever (AC240TS, Olympus, Tokyo, Japan). The typical scan size was $20 \times 20 \mu\text{m}^2$ and the scan rate was 0.5 Hz. Height difference profiles were determined from line profiles traced perpendicularly through the features of interest on the surfaces using Igor Pro MFP-3D software (Asylum Research, Santa Barbara, CA).

Immunostaining and fluorescence microscopy

Cells were fixed in 3.7% formaldehyde solution for 15 min at room temperature and, after four washes with PBS, cells were made permeable by incubation in 0.1% Triton X-100 for 30 min. Cells were again washed with PBS. All samples were blocked in 5% normal goat serum for 30 min. To detect phages bound to surfaces, samples were incubated with rabbit anti-fd (Sigma Aldrich, St Louis, MO) at 1 : 1000 dilution/PBST, and washed with PBST three times. Samples received the secondary stain goat Alexa fluorochrome-conjugated

anti-rabbit antibody (Molecular Probes, Eugene, OR), and were then incubated at 1 : 1000 dilution in PBST and washed three times with PBST. The fluorescence images were collected using an IX71 Fluorescence Microscope (Olympus, Tokyo, Japan). Areas, aspect ratios, elongation, orientation of the cells on various engineered phage and control surfaces were analyzed using NIH ImageJ (NIH, <http://rsb.info.nih.gov/ij/>).

Acknowledgements

This work was supported by the Hellman Family Faculty Fund (SWL), start-up funds from the Berkeley Nanoscience and Nano-engineering Institute at the University of California, Berkeley (SWL), and the Laboratory Directed Research and Development fund from the Lawrence Berkeley National Laboratory. We thank Mr Sean McFarland for help in editing this manuscript.

Notes and references

- 1 J. P. Bearinger, S. Terrettaz, R. Michel, N. Tirelli, H. Vogel, M. Textor and J. A. Hubbell, *Nat. Mater.*, 2003, **2**, 259–264.
- 2 D. Falconnet, G. Csucs, H. Michelle Grandin and M. Textor, *Biomaterials*, 2006, **27**, 3044–3063.
- 3 J. W. Lussi, D. Falconnet, J. A. Hubbell, M. Textor and G. Csucs, *Biomaterials*, 2006, **27**, 2534–2541.
- 4 J. W. Lussi, G. Csucs, M. Textor, J. A. Hubbell and G. Danuser, *Mol. Biol. Cell*, 2002, **13**, 1898.
- 5 D. Qin, Y. N. Xia and G. M. Whitesides, *Nat. Protoc.*, 2010, **5**, 491–502.
- 6 M. M. Stevens, M. Mayer, D. G. Anderson, D. B. Weibel, G. M. Whitesides and R. Langer, *Biomaterials*, 2005, **26**, 7636–7641.
- 7 Y. Xia and G. M. Whitesides, *Annu. Rev. Mater. Sci.*, 1998, **28**, 153–184.
- 8 J.-B. Kim, R. Ganesan, S. Y. Yoo, J.-H. Choi and S. Y. Lee, *Macromol. Rapid Commun.*, 2006, **27**, 1442–1445.
- 9 S. Y. Yoo, T.-I. Kim, S. Y. Lee, E. K. Kim, K. C. Keum, N. C. Yoo and W. M. Yoo, *Br. J. Ophthalmol.*, 2007, **91**, 722–727.
- 10 C. Czeisler, G. A. Silva, K. L. Niece, E. Beniash, D. A. Harrington, J. A. Kessler and S. I. Stupp, *Science*, 2004, **303**, 1352–1355.
- 11 S. Zhang, *Nat. Biotechnol.*, 2003, **21**, 1171–1178.
- 12 M. A. Biesalski, A. Knaebel, R. Tu and M. Tirrell, *Biomaterials*, 2006, **27**, 1259–1269.
- 13 J. C. Schense, J. Bloch, P. Aebischer and J. A. Hubbell, *Nat. Biotechnol.*, 2000, **18**, 415.
- 14 K. Y. Lee and D. J. Mooney, *Chem. Rev.*, 2001, **101**, 1869–1880.
- 15 D. J. Mooney, D. F. Baldwin, N. P. Suh, J. P. Vacanti and R. Langer, *Biomaterials*, 1996, **17**, 1417–1422.
- 16 E. R. Welsh and D. A. Tirrell, *Biomacromolecules*, 2000, **1**, 23–30.
- 17 C. T. S. Wong Po Foo, J. S. Lee, W. Mulyasmita, A. Parisi-Amon and S. C. Heilshorn, *Proc. Natl. Acad. Sci. U. S. A.*, 2009, **106**, 22067–22072.
- 18 A. J. Engler, S. Sen, H. L. Sweeney and D. E. Discher, *Cell*, 2006, **126**, 677–689.
- 19 S. Zhang, *Nat. Biotechnol.*, 2004, **22**, 151–152.
- 20 A. Merzlyak, S. Indrakanti and S.-W. Lee, *Nano Lett.*, 2009, **9**, 846–852.
- 21 A. Merzlyak and S.-W. Lee, *Bioconjugate Chem.*, 2009, **20**, 2300–2310.
- 22 A. B. Michael, K. Gagandeep, L. A. Lee, X. Fang, S. Jennifer, B. Rebecca, Z. Xiongfei, J. Maisie, P. R. Thomas, E. Todd and W. Qian, *ChemBioChem*, 2008, **9**, 519–523.
- 23 J. Rong, L. A. Lee, K. Li, B. Harp, C. M. Mello, Z. Niu and Q. Wang, *Chem. Commun.*, 2008, 5185–5187.
- 24 W.-J. Chung, A. Merzlyak, S. Y. Yoo and S.-W. Lee, *Langmuir*, 2010, **26**, 9885–9890.
- 25 W.-J. Chung, A. Merzlyak and S.-W. Lee, *Soft Matter*, 2010, **6**, 4454–4459.
- 26 D. J. Solis, S. R. Coyer, A. J. Garcia and E. Delamarche, *Adv. Mater.*, 2010, **22**, 111–114.

- 27 K. Nam, D. Kim, P. Yoo, C. Chiang, N. Meethong, P. Hammond, Y. Chiang and A. Belcher, *Science*, 2006, **312**, 885–888.
- 28 K. T. Nam, R. Wartena, P. J. Yoo, F. W. Liao, Y. J. Lee, Y.-M. Chiang, P. T. Hammond and A. M. Belcher, *Proc. Natl. Acad. Sci. U. S. A.*, 2008, **105**, 17227–17231.
- 29 P. J. Yoo, K. T. Nam, J. Qi, S.-K. Lee, J. Park, A. M. Belcher and P. T. Hammond, *Nat. Mater.*, 2006, **5**, 234–240.
- 30 P. Clark, P. Connolly, A. Curtis, J. Dow and C. Wilkinson, *J. Cell Sci.*, 1991, **99**, 73–77.
- 31 M. J. Dalby, M. O. Riehle, H. Johnstone, S. Affrossman and A. S. G. Curtis, *Cell Biol. Int.*, 2004, **28**, 229–236.
- 32 M. J. Dalby, M. O. Riehle, S. J. Yarwood, C. D. W. Wilkinson and A. S. G. Curtis, *Exp. Cell Res.*, 2003, **284**, 272–280.
- 33 M. J. Dalby, S. J. Yarwood, M. O. Riehle, H. J. H. Johnstone, S. Affrossman and A. S. G. Curtis, *Exp. Cell Res.*, 2002, **276**, 1–9.
- 34 F. Grinnell, *J. Cell Biol.*, 1994, **124**, 401–404.
- 35 R. G. Thakar, M. G. Chown, A. Patel, L. Peng, S. Kumar and T. A. Desai, *Small*, 2008, **4**, 1416–1424.
- 36 S. P. Massia and J. A. Hubbell, *J. Cell Biol.*, 1991, **114**, 1089–1100.
- 37 Y. Ito, *Soft Matter*, 2008, **4**, 46–56.
- 38 G. Maheshwari, G. Brown, D. A. Lauffenburger, A. Wells and L. G. Griffith, *J. Cell Sci.*, 2000, **113**(Pt 10), 1677–1686.
- 39 J. F. Pollock and K. Healy, in *Strategies in Regenerative Medicine*, ed. M. Santin, Springer, New York, 2009, pp. 97–154.
- 40 A. Khademhosseini, R. Langer, J. Borenstein and J. P. Vacanti, *Proc. Natl. Acad. Sci. U. S. A.*, 2006, **103**, 2480–2487.
- 41 A. B. Huber, A. L. Kolodkin, D. D. Ginty and J. F. Cloutier, *Annu. Rev. Neurosci.*, 2003, **26**, 509–563.
- 42 R. Milner and I. L. Campbell, *J. Neurosci. Res.*, 2002, **69**, 286–291.
- 43 J. T. Rutka, G. Apodaca, R. Stern and M. Rosenblum, *J. Neurosurg.*, 1988, **69**, 155–170.
- 44 S. F. Oster, A. Deiner, E. Birgbauer and D. W. Sretavan, *Semin. Cell Dev. Biol.*, 2004, **15**, 125–136.
- 45 I. Shirato, Y. Tomino, H. Koide and T. Sakai, *Cell Tissue Res.*, 1991, **266**, 1–10.
- 46 H. Makino, Y. Yamasaki and Z. Ota, *Nephron*, 1994, **66**, 189–199.
- 47 K. Hironaka, H. Makino, Y. Yamasaki and Z. Ota, *Renal Basement Membranes by Ultrahigh Resolution Scanning Electron Microscopy*, 1993.
- 48 M. N. Yousaf, B. T. Houseman and M. Mrksich, *Proc. Natl. Acad. Sci. U. S. A.*, 2001, **98**, 5992–5996.
- 49 W. A. Comisar, N. H. Kazmers, D. J. Mooney and J. J. Linderman, *Biomaterials*, 2007, **28**, 4409–4417.
- 50 E. A. Cavalcanti-Adam, A. Micoulet, J. Blümmel, J. Auernheimer, H. Kessler and J. P. Spatz, *Eur. J. Cell Biol.*, 2006, **85**, 219–224.